Supporting Information

Antifreeze-infused superhydrophobic surface with superb anti-icing and anti-frosting performance

Wei Weng[1,*], *Yueying Yu*[1,2], *Masanobu Naito*[1,2,*]

[1]Research Center for Macromolecules and Biomaterials, National Institute for Materials Science (NIMS), 1-2-1 Sengen, Tsukuba, Ibaraki, 305-0047, Japan

[2]Graduate School of Science and Technology, University of Tsukuba, 1-1-1 Tennodai, Tsukuba, Ibaraki, 305-8577, Japan

[*]Corresponding authors: weng.wei@nims.go.jp, naito.masanobu@nims.go.jp

Number of pages: 26

Number of figures: 16

Number of schemes: 0

Number of tables: 3

Table S1. Anti-icing and anti-frosting data of some reported superhydrophobic surfaces

Samples	FDT	IAS (kPa)	Complete frosting time
Nanograss-decorated Cu microcone arrays[1]		1.7	
Cu microcone arrays[1]		208.2	
Carbon nano-film[2]		474	
Etched Al plate[3]	130 s at -10 ºC	55.4	
ZnO nanorods on steel plate[4]		6	
Micropillars of CNT/PDMS[5]	309 s at -20 ºC	84	
Nanowires on PDMS microcone arrays[6]		44.1	
Polyurethane with SiO_2 nanoparticles[7]	2137 s at -20 ºC	21.2	
Nanostructured woven wire cloths[8]		180	
PTFE/nanodiamond/MXene composite[9]	403 s at -20 ºC	56.4	
Carbon nanowire-coated carbon cloths[10]	3600 s at -15 ºC		
MOFs on cotton fabrics[11]	118.6 s at -20 ºC		
Dual-scale rough Al plate[12]	4896 s at -19 ºC	78	
Polydopamine/PDMS/SiO_2 composite[13]	1800 s at -15 ºC		
SiO_2/TiO_2/epoxy composite[14]	801 s at -15 ºC		
PDMS/PTFE/SiO_2 composite[15]	441 s at -15 ºC	27	
Nanoparticle-modified polyurethane[16]	213 s at -15 ºC		
Hydrophobic CB on etched Al alloy[17]	300 s at -30 ºC	13.8	300 s at -10 ºC
Micro/nanostructured AlSi10Mg alloy[18]			1800 s at -15 ºC
PUA-coated patterned Ti alloy[19]			360 s at -9 ºC
Dual-scale hierarchical 7075 Al alloy[20]			5280 s at -7 ºC
Silicon microposts[21]			540 s at -10 ºC

PDMS: polydimethylsiloxane; CNT: carbon nanotube; PTFE: poly(tetrafluoroethylene); MOFs: metal-organic frameworks; CB: carbon black; PUA: polyurethane acrylate

Table S2. Anti-icing and anti-frosting data of some reported SLIPS

Samples	FDT	IAS (kPa)	Complete frosting time
Perfluoropolyether-infused etched Al plate[3]	60 s at -10 ºC	24.1	
Perfluoropolyether-infused AlSi10Mg alloy[18]			600 s at -13 ºC
Perfluoropolyether-infused Si microposts[21]			720 s at -10 ºC
Silicone oil-infused microporous silica/PDMS[22]		45	2400 s at -10 ºC
Perfluoropolyether-infused nanoengineered Cu[23]			267 s at -10 ºC
Silicone oil-infused CNT/polyurethane/styrene composite[24]		58	
Silicone oil-infused silica nanoparticle-filled epoxy micropillars[25]		2	
Silicone oil-infused epoxy micropillars[25]		25	
Silicone oil-infused silica/epoxy/PDMS[26]	652 s at -10 ºC	5.5	
Perfluoropolyether-infused Mg plate with fish scale structure[27]	1532 s at -20 ºC	25	
Silicone oil-infused sepiolite/GO/ZIF-8-coated Mg alloy[28]	310 s at -20 ºC	45	
Perfluoropolyether-infused CuO-coated copper foil[29]	728 s at -10 ºC		
Silicone oil-infused etched Mg alloy[30]	896 s at -10 ºC	48.1	

GO: graphene oxide

Table S3. Anti-icing and anti-frosting data of some reported antifreeze-based surfaces

Samples	FDT	IAS (kPa)	Complete frosting time
EG in PEI/SiO_2[31]		7	
EG in PVA covered by SHPO Cu mesh[32]	25200 s at -10 ºC	1.1 & 0.011	25200 s at -10 ºC
PG film[33]			19200 s at -10 ºC
PG drop arrays[33]			28800 s at -10 ºC
PG in nylon[23]			5400 s at -10 ºC
PG in nylon covered by hydrobead coating[23]			6000 s at -10 ºC
PG in nylon covered by PC nanoporous membrane[34]			12000 s at -10 ºC 3000 s at -20 ºC 1200 s at -30 ºC
PG in PAA/cotton[35]		0.042	

PEI: polyethylenimine; PVA: polyvinyl alcohol; SHPO: superhydrophobic; PC: polycarbonate

(1) Pan, R.; Zhang, H.; Zhong, M. Triple-Scale Superhydrophobic Surface with Excellent Anti-Icing and Icephobic Performance via Ultrafast Laser Hybrid Fabrication. *ACS Appl. Mater. Interfaces* **2021**, *13*, 1743–1753.

(2) Xu, Y.; Zhang, G.; Li, L.; Xu, C.; Lv, X.; Zhang, H.; Yao, W. Icephobic Behaviors of Superhydrophobic Amorphous Carbon Nano-Films Synthesized from a Flame Process. *J. Colloid Interface Sci.* **2019**, *552*, 613–621.

(3) Zhang, B.; Xu, W.; Xia, D. H.; Fan, X.; Duan, J.; Lu, Y. Comparison Study of Self-Cleaning, Anti-Icing, and Durable Corrosion Resistance of Superhydrophobic and Lubricant-Infused Ultraslippery Surfaces. *Langmuir* **2021**, *37*, 11061–11071.

(4) Balordi, M.; Pini, F.; Santucci de Magistris, G. Superhydrophobic Ice-Phobic Zinc Surfaces. *Surf. Interfaces* **2022**, *30*, 101855.

(5) Sun, Y.; Wang, Y.; Liang, W.; He, L.; Wang, F.; Zhu, D.; Zhao, H. In Situ Activation of Superhydrophobic Surfaces with Triple Icephobicity at Low Temperatures. *ACS Appl. Mater. Interfaces* **2022**, *14*, 49352–49361.

(6) Chen, C.; Tian, Z.; Luo, X.; Jiang, G.; Hu, X.; Wang, L.; Peng, R.; Zhang, H.; Zhong, M. Micro-Nano-Nanowire Triple Structure-Held PDMS Superhydrophobic Surfaces for Robust Ultra-Long-Term Icephobic Performance. *ACS Appl. Mater. Interfaces* **2022**, *14*, 23973–23982.

(7) Zhao, Y.; Hao, T.; Wu, W.; Meng, Y.; Cao, X.; Zhang, Q.; She, W.; You, J.; Shi, D.; Jiang, T. A Novel Moisture-Controlled Siloxane-Modified Hyperbranched Waterborne Polyurethane for Durable Superhydrophobic Coatings. *Appl. Surf. Sci.* **2022**, *587*, 152446.

(8) Wood, M. J.; Brock, G.; Debray, J.; Servio, P.; Kietzig, A. M. Robust Anti-Icing Surfaces Based on Dual Functionality─Microstructurally-Induced Ice Shedding with Superimposed Nanostructurally-Enhanced Water Shedding. *ACS Appl. Mater.*

Interfaces **2022**, *14*, 47310–47321.

(9) Zhao, Y.; Yan, C.; Hou, T.; Dou, H.; Shen, H. Multifunctional Ti3C2Tx MXene-Based Composite Coatings with Superhydrophobic Anti-Icing and Photothermal Deicing Properties. *ACS Appl. Mater. Interfaces* **2022**, *14*, 26077–26087.

(10) Xie, Z.; Wang, H.; Geng, Y.; Li, M.; Deng, Q.; Tian, Y.; Chen, R.; Zhu, X.; Liao, Q. Carbon-Based Photothermal Superhydrophobic Materials with Hierarchical Structure Enhances the Anti-Icing and Photothermal Deicing Properties. *ACS Appl. Mater. Interfaces* **2021**, *13*, 48308–48321.

(11) Li, W.; Zhang, Y.; Yu, Z.; Zhu, T.; Kang, J.; Liu, K.; Li, Z.; Tan, S. C. In Situ Growth of a Stable Metal-Organic Framework (MOF) on Flexible Fabric via a Layer-by-Layer Strategy for Versatile Applications. *ACS Nano* **2022**, *16*, 14779–14791.

(12) Lo, T. N. H.; Hong, S. W.; Hwang, H. S.; Park, I. Facile Synthesis of Fluorinated Polysilazanes and Their Durable Icephobicity on Rough Al Surfaces. *Polymers (Basel).* **2022**, *14*, 330.

(13) Zhao, Z.; Zhang, Q.; Song, X.; Chen, J.; Ding, Y.; Wu, H.; Guo, S. Versatile Melanin-Like Coatings with Hierarchical Structure toward Personal Thermal Management, Anti-Icing/Deicing, and UV Protection. *ACS Appl. Mater. Interfaces* **2023**, *15*, 3522–3533.

(14) Xin, L.; Li, P.; Li, H.; Sun, W.; Zhang, C.; Zhang, K.; Yin, X.; Yu, S. Fabrication of Decoupling Coatings with Robustness and Superhydrophobicity for Anti-Icing and Anti-Corrosion Applications. *J. Mater. Sci.* **2023**, *58*, 6038–6054.

(15) Patil, A. H.; Trinh, N. Le; Do, H.; Gaiji, H.; Kang, Y.; Lee, J.; Chung, C.; Lee, H. B. R. Facile Approach for Designing Icephobic Coatings Using Polymers/Silica Nanoparticle Composites via Self-Formation of Superhydrophobic Surfaces. *Adv. Mater. Interfaces* **2024**, *11*.

(16) Li, H.; Xin, L.; Gao, J.; Shao, Y.; Zhang, Z.; Ren, L. Underwater Bionic Self-Healing Superhydrophobic Coating with the Synergetic Effect Of Hydrogen Bonds and Self-Formed Bubbles. *Small* **2024**, *20*, 2309012.

(17) Zhao, Y.; Liu, W.; Du, Y.; Tong, J.; Xie, H.; Wu, T.; Qu, J. Anti-Frosting and Defrosting Fins with Hierarchical Interlocking Structure for Enhancing Energy Utilization Efficiency of Heat Exchanger. *Small* **2024**, *2405424*, 1–11.

(18) Zhao, H.; Ye, H.; Fazle Rabbi, K.; Wang, X.; Miljkovic, N.; Ho, J. Y. Micro- and Nanoengineered Metal Additively Manufactured Surfaces for Enhanced Anti-Frosting Applications. *ACS Appl. Mater. Interfaces* **2024**, *16*, 35697–35715.

(19) Dai, Q.; Chen, L.; Pan, J.; Shi, L.; Liu, D.; Huang, W.; Wang, X. Rapid Surface Texturing to Achieve Robust Superhydrophobicity, Controllable Droplet Impact, and Anti-Frosting Performances. *Friction* **2024**, *12*, 291–304.

(20) Liu, D.; Liu, R.; Cao, L.; Wang, L.; Saeed, S.; Wang, Z.; Bryanston-Cross, P. Superhydrophobic Antifrosting 7075 Aluminum Alloy Surface with Stable Cassie-Baxter State Fabricated through Direct Laser Interference Lithography and Hydrothermal Treatment. *Langmuir* **2024**, *40*, 950–959.

(21) Rykaczewski, K.; Anand, S.; Subramanyam, S. B.; Varanasi, K. K. Mechanism of Frost Formation on Lubricant-Impregnated Surfaces. *Langmuir* **2013**, *29*, 5230–5238.

(22) Wen, S. F.; Wang, Y. M.; Zhang, Z. M.; Liu, Y. L. Application of Anti-Icing Coating Based on Adsorption of Functional Substances by Microporous Sphere. *Prog. Org. Coatings* **2019**, *137*, 105320.

(23) Sun, X.; Damle, V. G.; Liu, S.; Rykaczewski, K. Bioinspired Stimuli-Responsive and Antifreeze-Secreting Anti-Icing Coatings. *Adv. Mater. Interfaces* **2015**, *2*, 1400479.

(24) Liu, X.; Chen, H.; Zhao, Z.; Yan, Y.; Zhang, D. Slippery Liquid-Infused Porous Electric Heating Coating for Anti-Icing and de-Icing Applications. *Surf. Coatings*

Technol. **2019**, *374*, 889–896.

(25) Wong, W. S. Y.; Hegner, K. I.; Donadei, V.; Hauer, L.; Naga, A.; Vollmer, D. Capillary Balancing: Designing Frost-Resistant Lubricant-Infused Surfaces. *Nano Lett.* **2020**, *20*, 8508–8515.

(26) Zhou, L.; Liu, A.; Tang, J.; Han, Y.; Kang, J.; Li, Y.; Kuai, S.; Xue, X.; Chen, N.; Liu, H. Mechanically Robust Liquid-Embedded Coating with Anti-Icing/Deicing Durability. *Colloids Surfaces A Physicochem. Eng. Asp.* **2023**, *674*, 131924.

(27) Song, X.; Hou, Y.; Zhang, X.; Zhao, Y.; Wu, Y.; Liu, M.; Guo, Z. Multiplex Biomimetic SLIPS With Super-Lubricity to Multiphase Matters. *Small* **2025**, *21*, 2407530.

(28) Li, B.; Huang, K.; Xue, S.; Liu, W.; Li, J. Robust Slippery Liquid-Infused Porous Surfaces with Fast Self-Replenishment Properties for Anticontaminant, Anti-Icing, and Anticorrosion Applications on Magnesium Alloys. *ACS Appl. Mater. Interfaces* **2025**, *17*, 19105–19116.

(29) Gou, X.; Guo, Z. Facile Fabrication of Slippery Lubricant-Infused CuO-Coated Surfaces with Different Morphologies for Efficient Water Collection and Excellent Slippery Stability. *Langmuir* **2020**, *36*, 8983–8992.

(30) Liu, C.; Li, Y.; Lu, C.; Liu, Y.; Feng, S.; Liu, Y. Robust Slippery Liquid-Infused Porous Network Surfaces for Enhanced Anti-Icing/Deicing Performance. *ACS Appl. Mater. Interfaces* **2020**, *12*, 25471–25477.

(31) Yamazaki, T.; Tenjimbayashi, M.; Manabe, K.; Moriya, T.; Nakamura, H.; Nakamura, T.; Matsubayashi, T.; Tsuge, Y.; Shiratori, S. Antifreeze Liquid-Infused Surface with High Transparency, Low Ice Adhesion Strength, and Antifrosting Properties Fabricated through a Spray Layer-by-Layer Method. *Ind. Eng. Chem. Res.* **2019**, *58*, 2225–2234.

(32) Liu, F.; Wang, Z.; Pan, Q. Intelligent Icephobic Surface toward Self-Deicing Capability. *ACS Sustain. Chem. Eng.* **2020**, *8*, 792–799.

(33) Sun, X.; Damle, V. G.; Uppal, A.; Linder, R.; Chandrashekar, S.; Mohan, A. R.; Rykaczewski, K. Inhibition of Condensation Frosting by Arrays of Hygroscopic Antifreeze Drops. *Langmuir* **2015**, *31*, 13743–13752.

(34) Sun, X.; Rykaczewski, K. Suppression of Frost Nucleation Achieved Using the Nanoengineered Integral Humidity Sink Effect. *ACS Nano* **2017**, *11*, 906–917.

(35) Yao, X.; Chen, B.; Morelle, X. P.; Suo, Z. Anti-Icing Propylene-Glycol Materials. *Extrem. Mech. Lett.* **2021**, *44*, 101225.

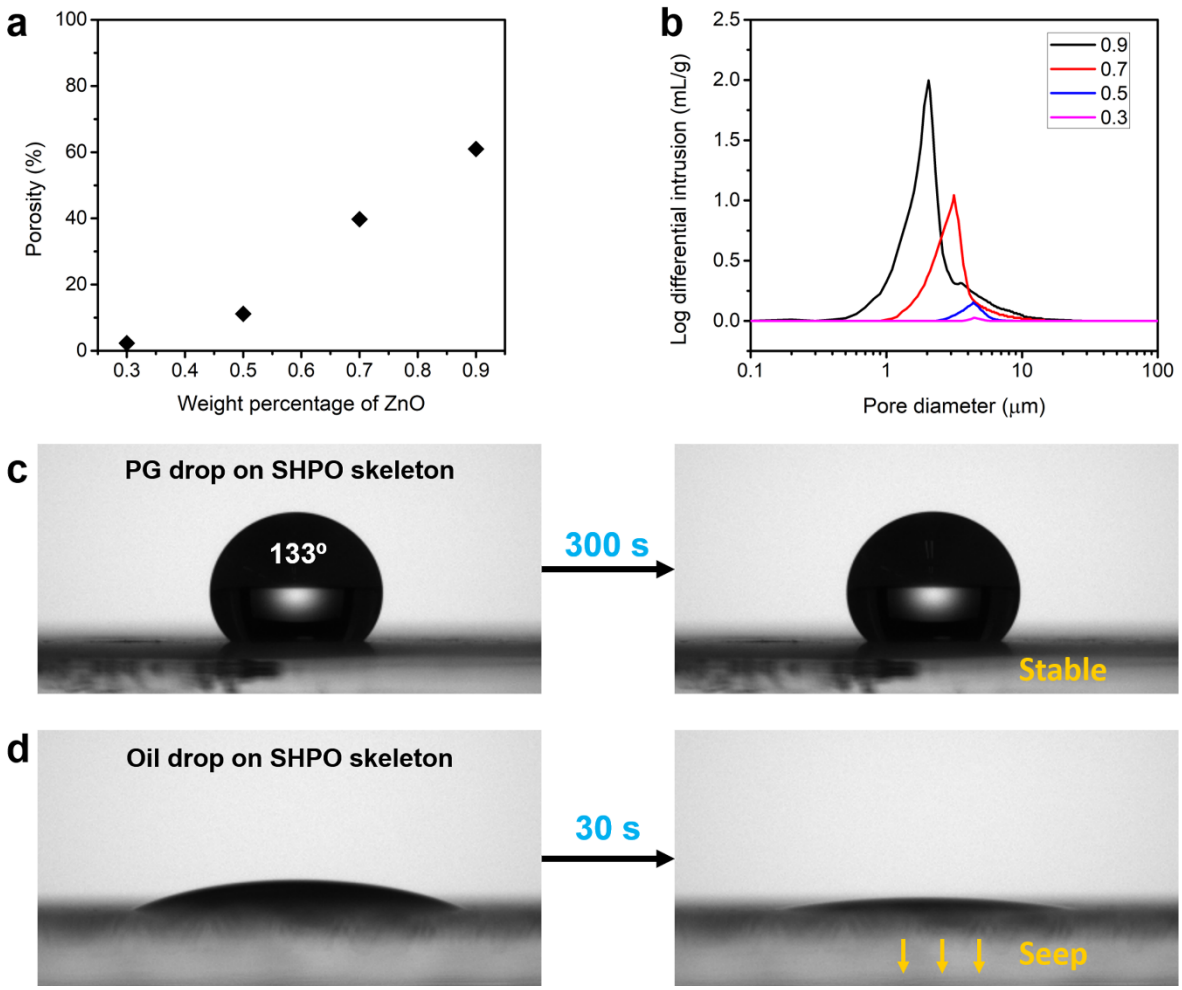

Figure S1. a) Dependence of porosity on weight percentage of ZnO in ZnO/PDMS skeletons. b) Distribution of pore size of ZnO/PDMS skeletons at various weight percentages of ZnO. c) PG drop (5 μL) and d) silicone oil drop (5 μL) sitting on superhydrophobic (SHPO) skeleton with a ZnO:PDMS weight ratio of 9:1.

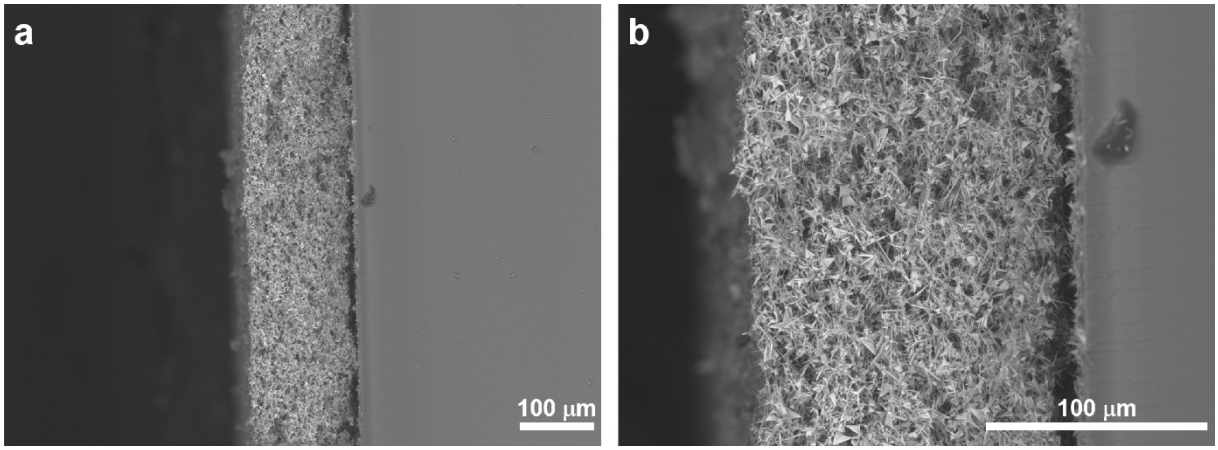

Figure S2. Cross-sectional SEM images of superhydrophobic skeleton with a) a low magnificaiton and b) a high magnification.

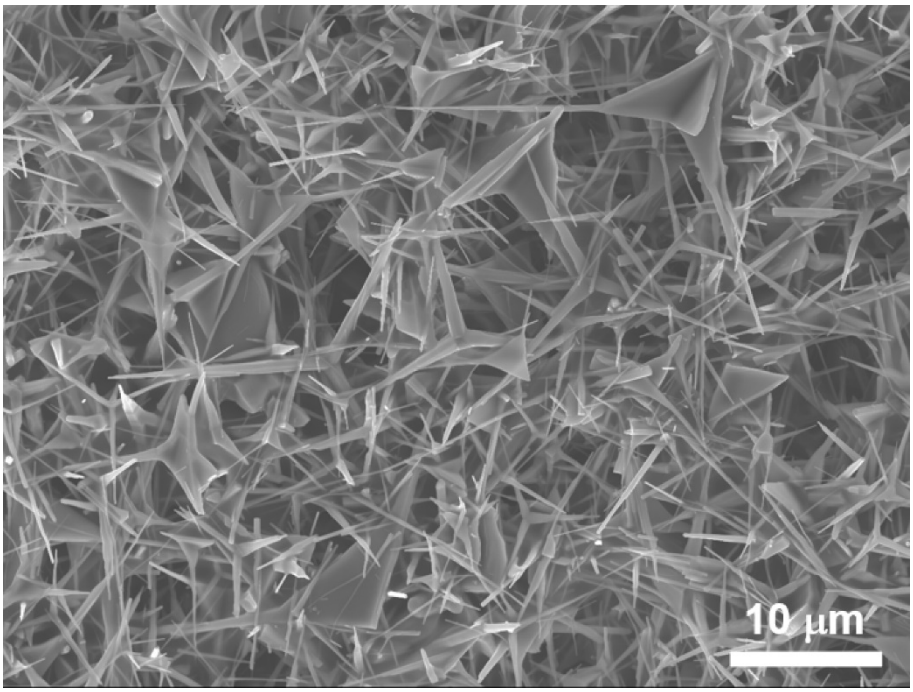

Figure S3. FESEM image of superhydrophobic skeleton.

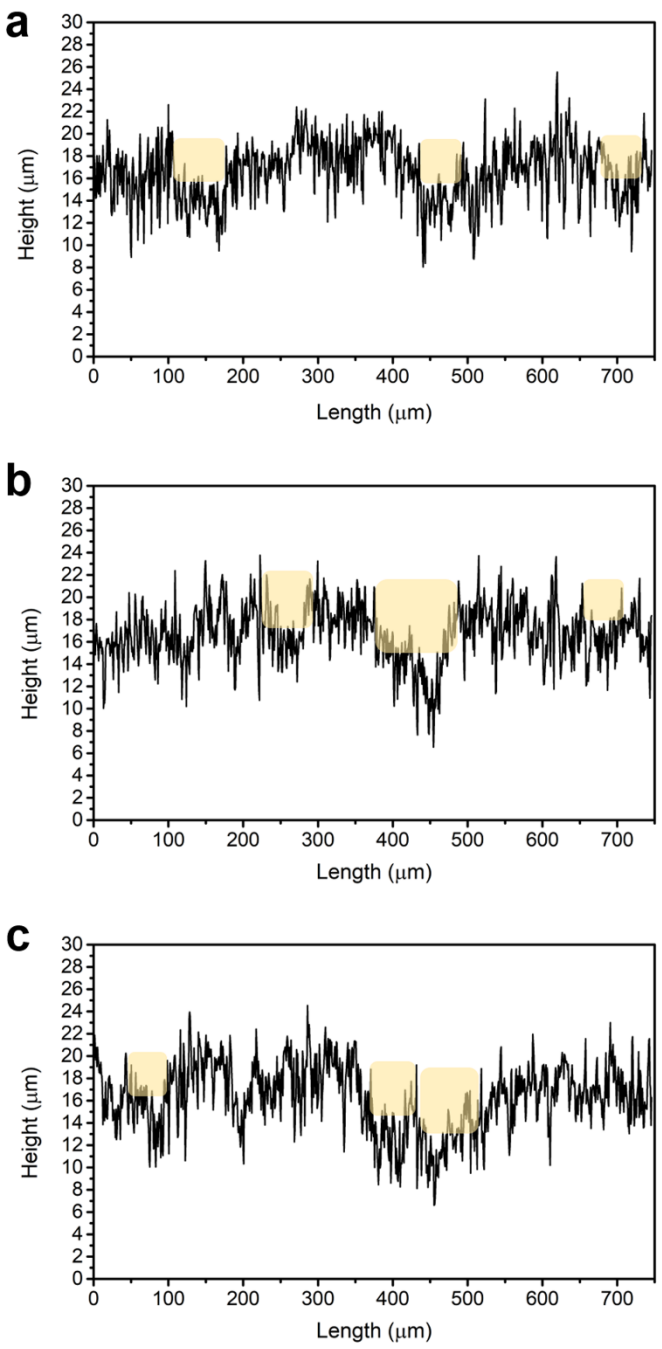

Figure S4. a), b) and c) Surface height profiles of superhydrophobic skeleton at different zones. Pores that could entrap air are filled with yellow color.

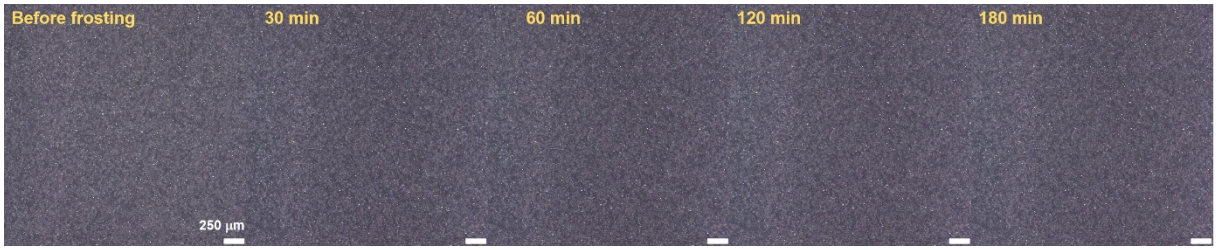

Figure S5. Evolution of PG-infused skeleton at -10 ºC with ambient conditions of 42% of relative humidity and 10 ºC by laser scanning confocal microscopy. The sample was horizontally placed. The detect area is the circle by dash lines in Figure 3c.

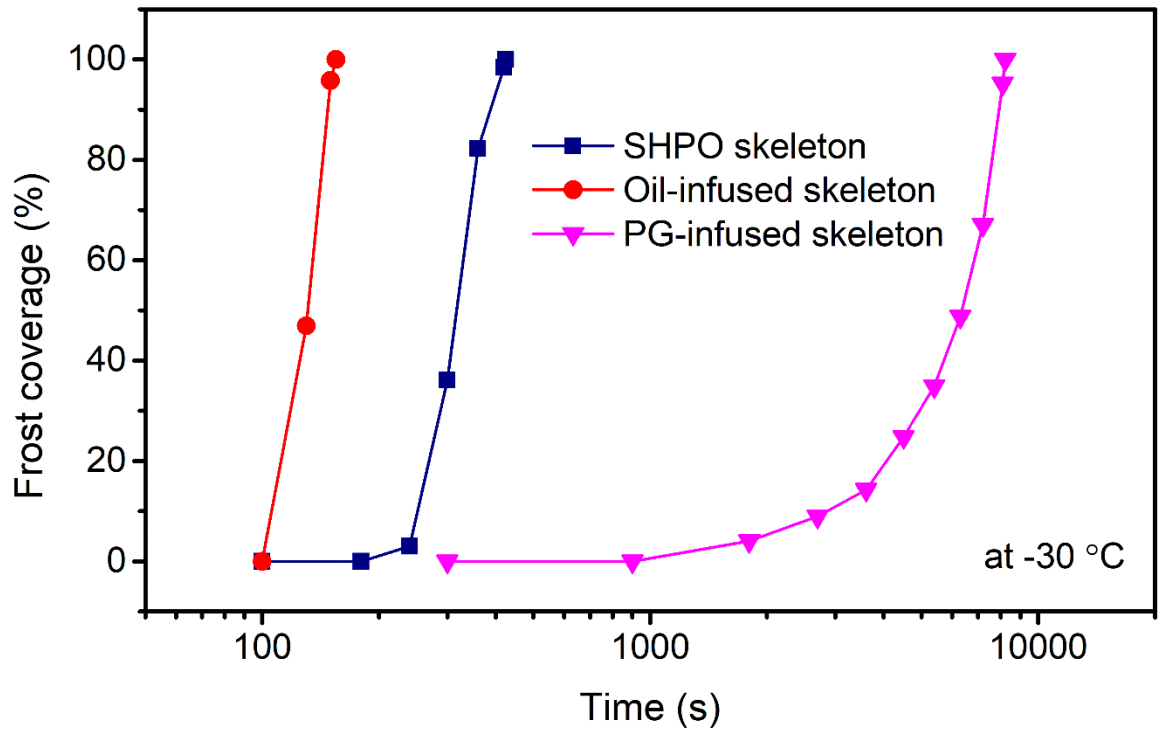

Figure S6. Plots of frost coverage versus frosting time for superhydrophobic (SHPO) skeleton, oil-infused skeleton, and PG-infused skeleton at -30 ºC.

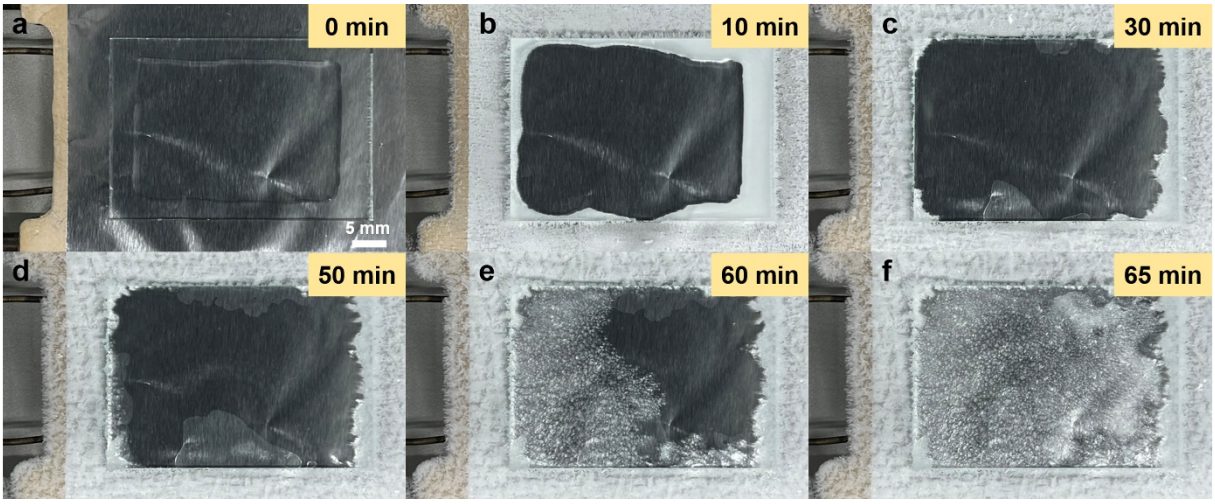

Figure S7. Photos of frosting of PG film on glass slide at -30 ºC.

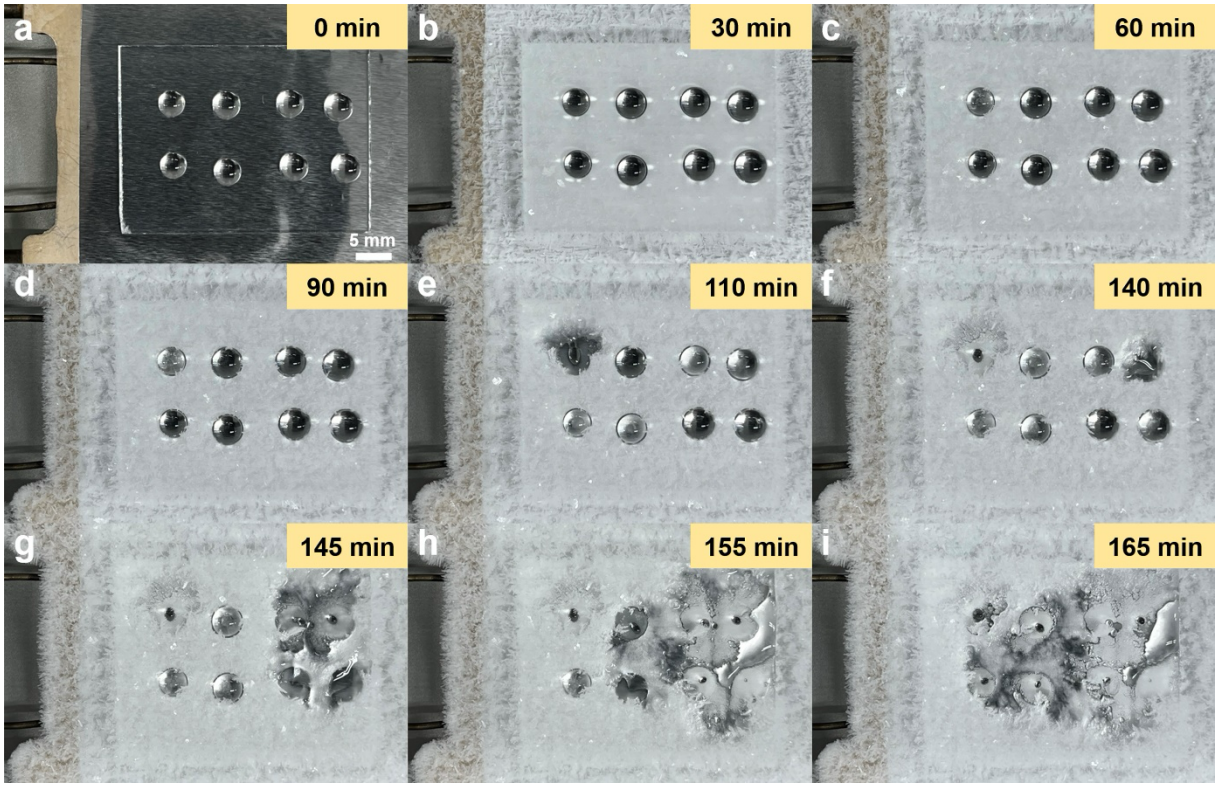

Figure S8. Photos of frosting of PG drop arrays on flat PDMS film at -30 ºC.

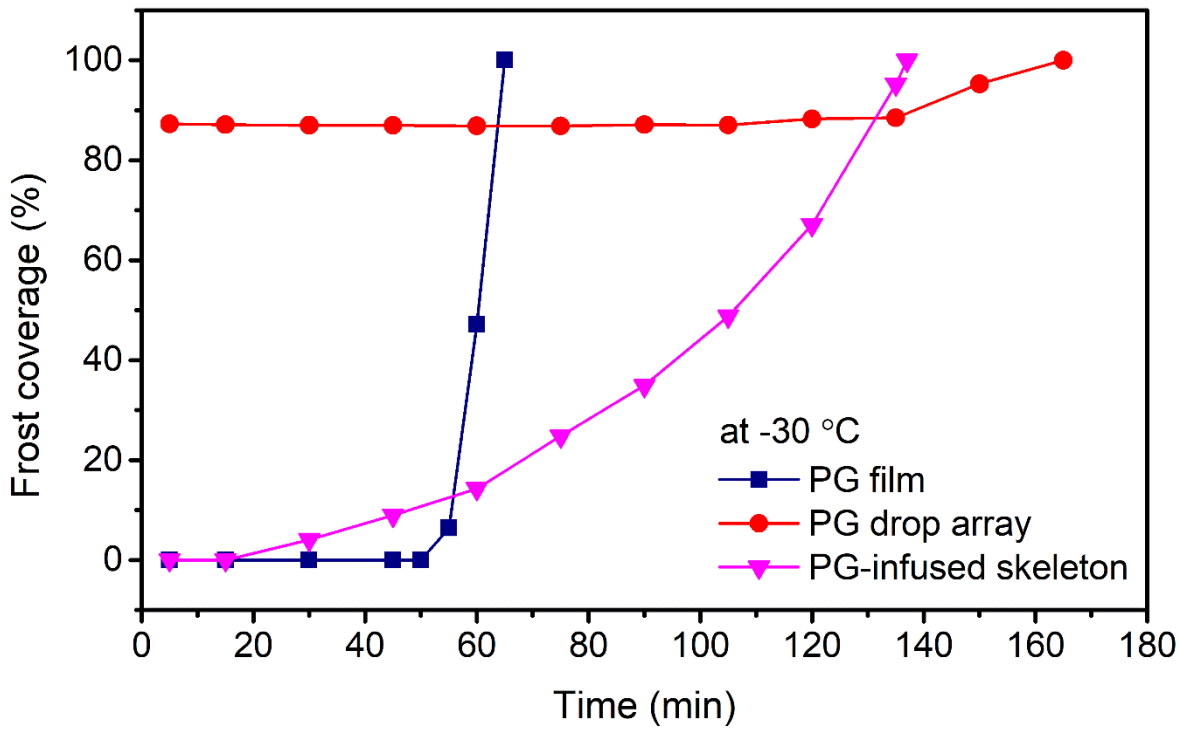

Figure S9. Plots of frost coverage versus frosting time for PG film, PG drop arrays, and PG-infused skeleton at -30 ºC.

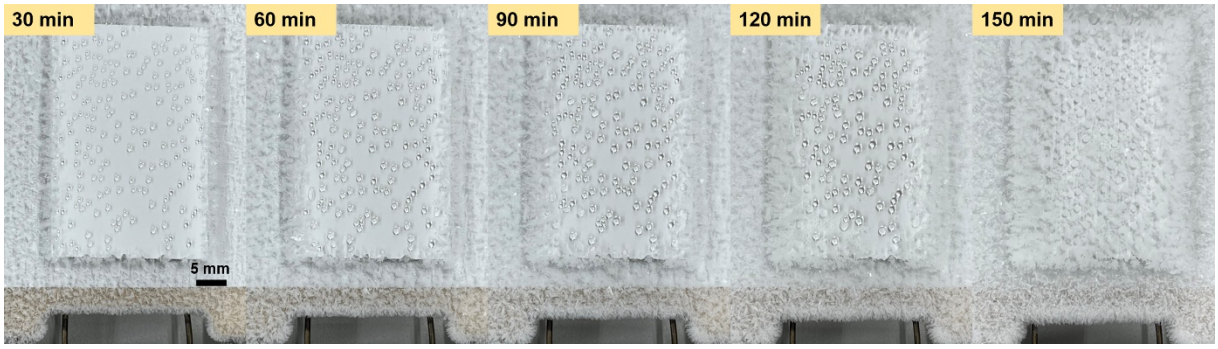

Figure S10. Photos of frosting of EG-infused skeleton at -30 ºC.

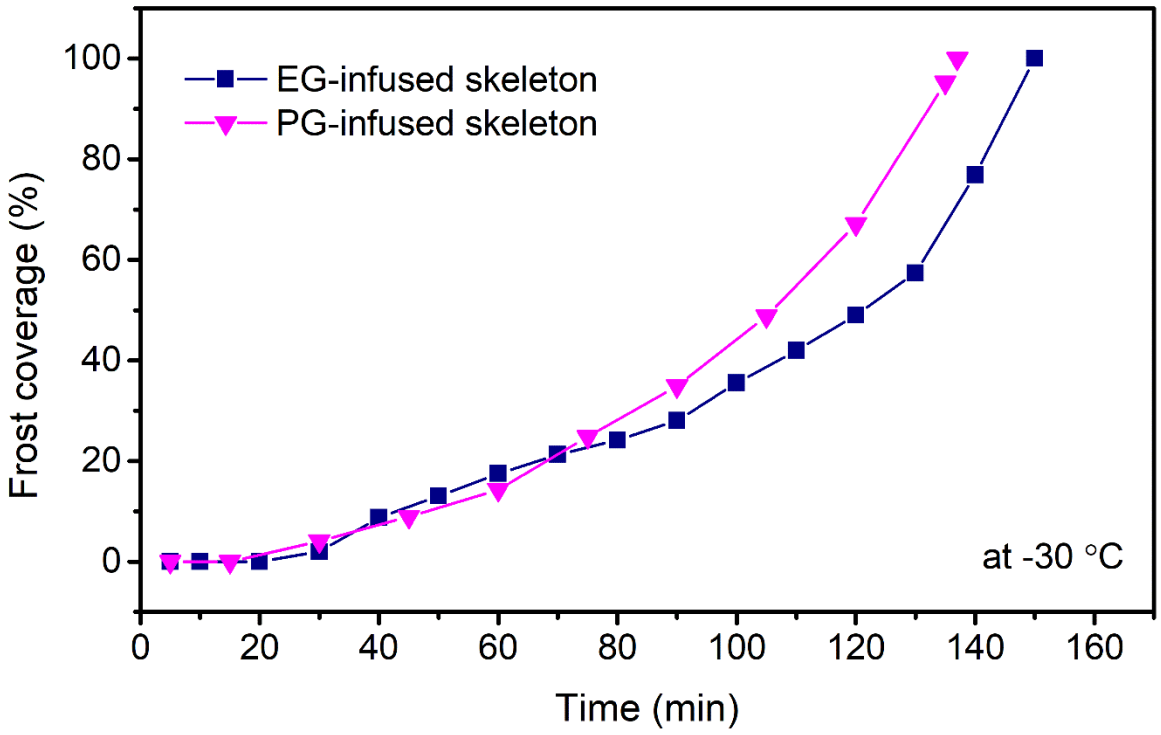

Figure S11. Plots of frost coverage versus frosting time for EG-infused skeleton and PG-infused skeleton at -30 ºC.

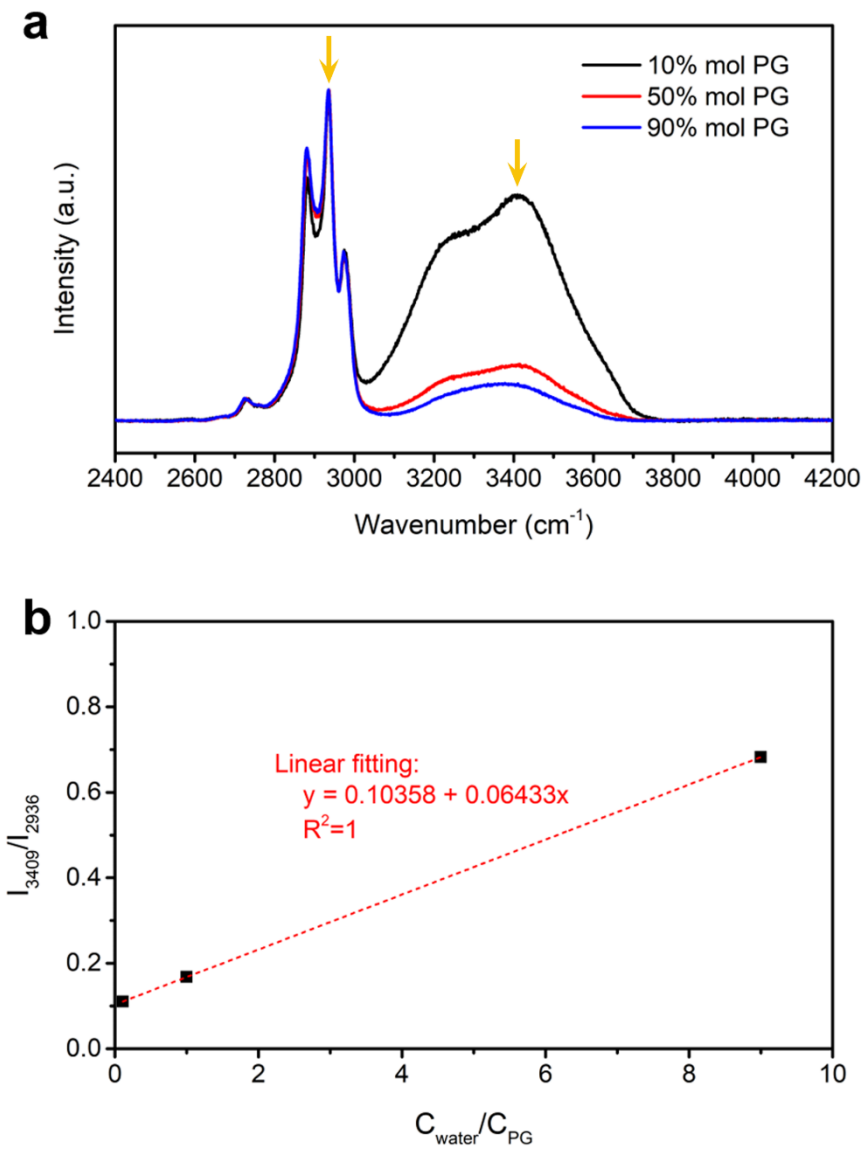

Figure S12. a) Raman spectra of water/PG solutions with 10%, 50%, and 90% mol of PG. b) Peak intensity ratio of OH stretching vibrations to CH_2 stretching vibrations (I_{3409}/I_{2936}) as a function of molar ratio of water to PG (C_{water}/C_{PG}).

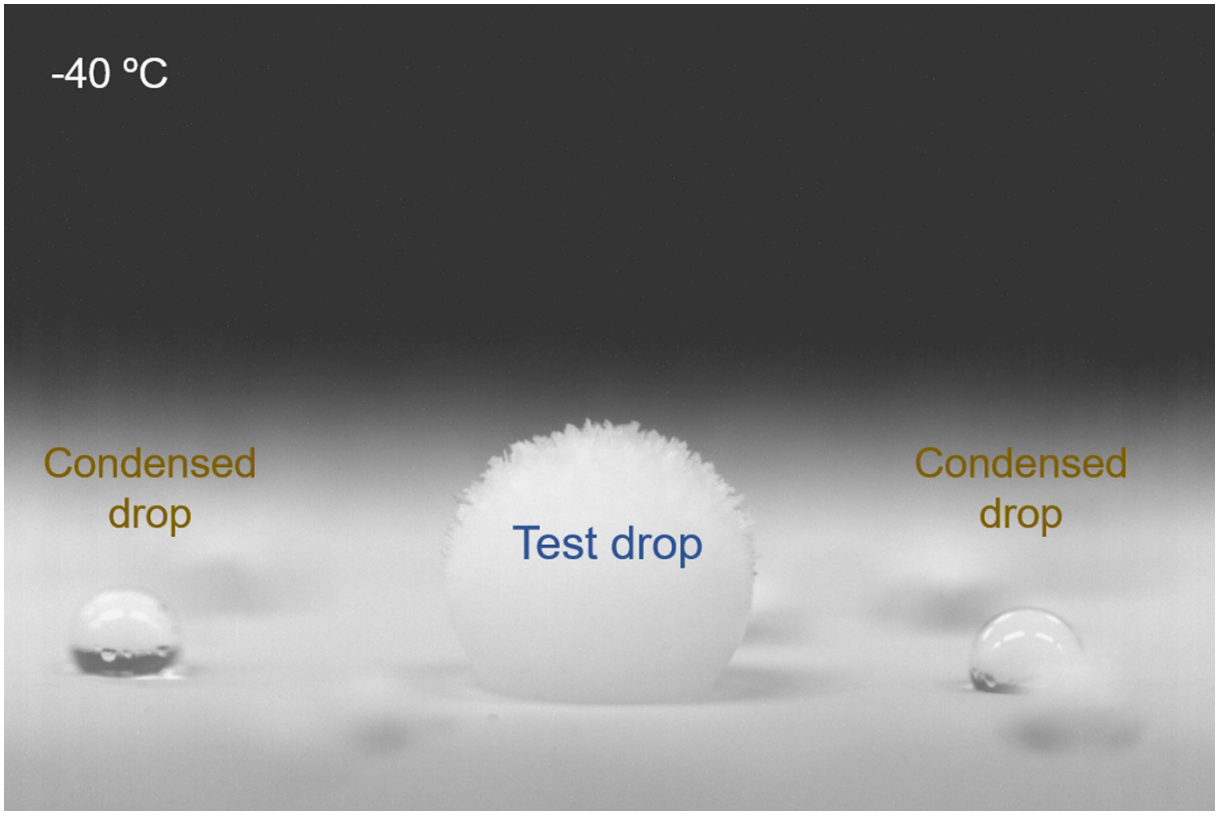

Figure S13. Test water drop and condensed drops on PG-infused skeleton at -40 ºC under INT test.

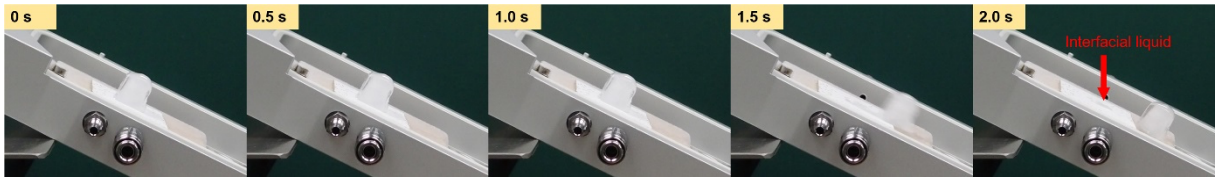

Figure S14. Photos of sliding of an ice cube on a 25º titled surface (-10 ºC) by its own gravity.

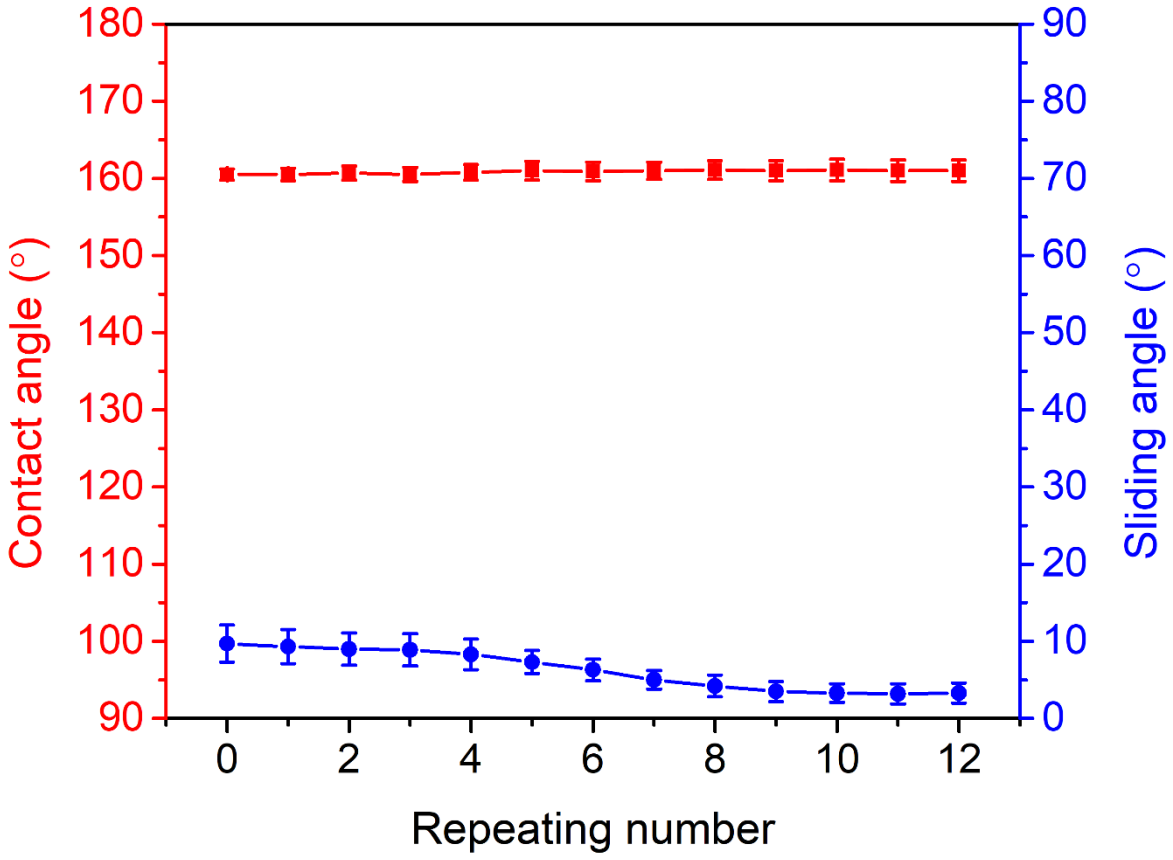

Figure S15. CAs and SAs of water drops (10 μL) on PG-infused skeleton after each test during repeating frosting at -10 ºC.

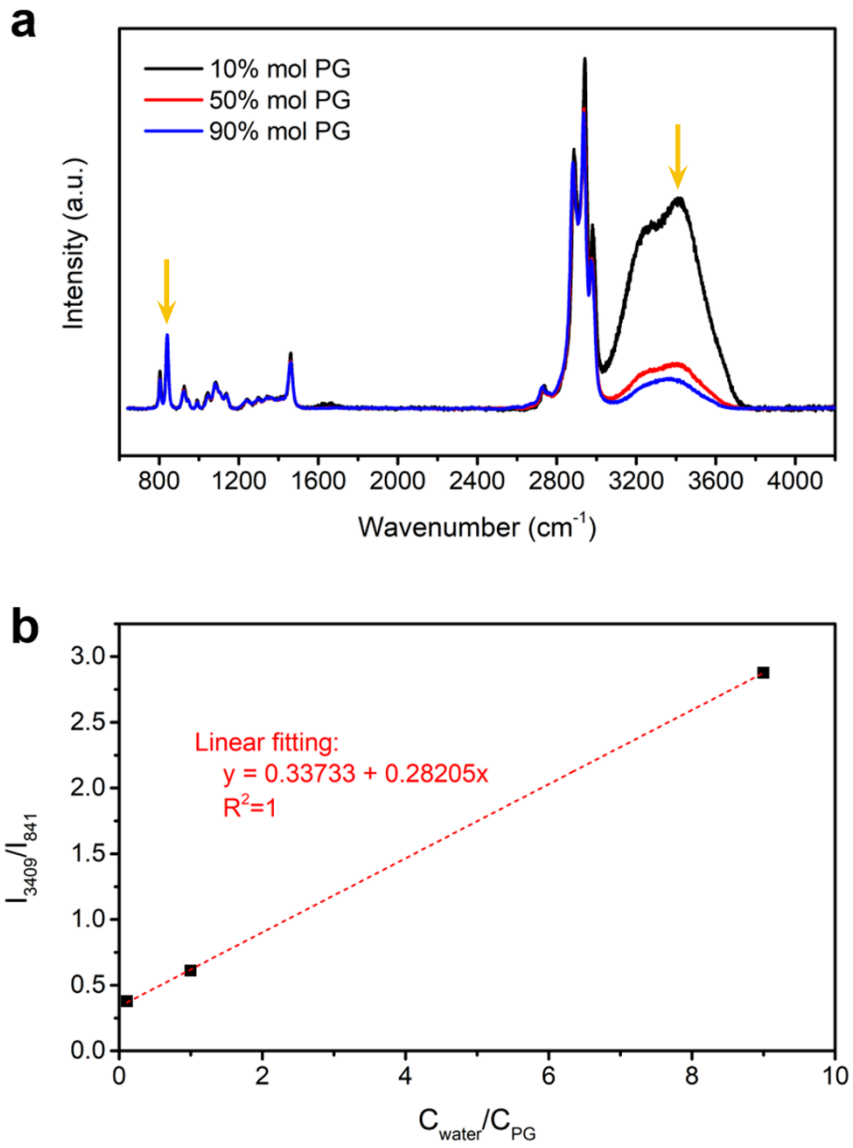

Figure S16. a) Raman spectra of water/PG solutions with 10%, 50%, and 90% mol of PG. b) Peak intensity ratio of OH stretching vibrations to *gauche*-conformers (I_{3409}/I_{841}) as a function of molar ratio of water to PG (C_{water}/C_{PG}).